energies

Article

Three-Dimensional Geological Modeling and Resource Estimation of Hot Dry Rock in the Gonghe Basin, Qinghai Province

Guilin Zhu [1,2], Linyou Zhang [2,*], Zhihui Deng [2], Qingda Feng [2], Zhaoxuan Niu [2] and Wenhao Xu [2]

[1] Key Laboratory of Groundwater Resources and Environment, Jilin University, Changchun 130012, China
[2] Center for Hydrogeology and Environmental Geology Survey, Tianjin 300300, China; fengqingda@mail.cgs.gov.cn (Q.F.)
* Correspondence: zhanglinyou@mail.cgs.gov.cn

Abstract: The Gonghe Basin, situated on the northeastern margin of the Qinghai–Tibet Plateau, is a strike-slip pull-apart basin that has garnered considerable attention for its abundant high-temperature geothermal resources. However, as it is located far from the Himalayan geothermal belt, research on the geothermal resources in the Gonghe Basin has mainly focused on the heat source mechanism, with less attention given to the distribution and resource potential of hot dry rock. In this project, a comprehensive approach combining geological surveys, geophysical exploration, geochemical investigations, and deep drilling was employed to analyze the stratigraphic structure and lithological composition of the Gonghe Basin, establish a basin-scale three-dimensional geological model, and identify the lithological composition and geological structures within the basin. The model revealed that the target reservoirs of hot dry rock in the Gonghe Basin exhibit a half-graben undulation pattern, with burial depths decreasing from west to east and reaching a maximum depth of around 7000 m. Furthermore, the distribution of the temperature field in the area was determined, and the influence of temperature on rock density and specific heat was investigated to infer the thermal properties of the deep reservoirs. The Qiabuqia region, situated in the central-eastern part of the basin, was identified as a highly favorable target area for hot dry rock exploration and development. The volume method was used to evaluate the potential of hot dry rock resources in the Gonghe Basin, which was estimated to be approximately 4.90×10^{22} J, equivalent to 1.67×10^{12} t of standard coal, at depths of up to 10 km.

Keywords: geothermal resource; HDR; three-dimensional geological model; Gonghe Basin

Citation: Zhu, G.; Zhang, L.; Deng, Z.; Feng, Q.; Niu, Z.; Xu, W. Three-Dimensional Geological Modeling and Resource Estimation of Hot Dry Rock in the Gonghe Basin, Qinghai Province. *Energies* **2023**, *16*, 5871. https://doi.org/10.3390/en16165871

Academic Editors: Javier F. Urchueguía and Fangming Jiang

Received: 19 June 2023
Revised: 8 July 2023
Accepted: 20 July 2023
Published: 8 August 2023

1. Introduction

With the rapid depletion of fossil fuels and the accompanying environmental concerns they pose, alternative energy sources such as solar energy, wind energy, and geothermal energy have increasingly emerged as viable options [1]. Geothermal energy is a renewable and green energy source that causes almost zero pollution to the environment during its development and utilization process. High-temperature geothermal energy can be used to generate electricity. Compared to other new energy sources, geothermal energy resources have the advantages of good thermal continuity, being unaffected by seasonal changes, climate, and day and night restrictions [2]. The International Energy Agency aims at a world-wide increase in renewable electricity production using geothermal energy from presently about 10 GWe to 140–160 GWe installed capacity by 2050 [3,4].

Hot dry rock (HDR) is a type of geothermal resource that is typically stored in rocks with a sufficiently high temperature (>180 °C) but with low porosity and permeability, resulting in insufficient fluids for effective heat transfer [5]. China has abundant HDR resources, with a total resource potential of 2.09×10^7 EJ at depths of 3–10 km [6]. If 2% is taken as the recoverable coefficient, the exploitable HDR energy in the depth range of

3~10 km was conservatively estimated to be 4.2×10^5 EJ, which approximately amounts to 2870 times the annual energy consumption of China in 2020.

Although the development and utilization of HDR has been put into practice since the 1970s [7], the dense and almost porous-free nature of HDR means that large-scale fracture networks need to be created through hydraulic fracturing to enable the circulation of heat transfer fluids (mainly water) at a certain flow rate before the heat energy can be extracted. During the extraction process, HDR may trigger earthquakes [8] or suffer from issues such as poor connectivity and significant losses of circulating fluid [9]. Therefore, prior to the development of HDR engineering, it is necessary to investigate the regional geological conditions, establish a three-dimensional geological model, and determine the geological structure and geothermal distribution in order to avoid geological risks and financial waste during the development process.

Due to the influence of the Indian plate subducting beneath the Eurasian plate, the Qinghai–Tibet Plateau in China has abundant geothermal resources, which are mainly concentrated in the southwestern region. The geothermal activity in the northeastern region has not been clearly demonstrated, and it has long been believed that the geothermal resources in this area are relatively scarce. In 2018, the GR1 drilling project carried out in the Gonghe Basin, located in the northeastern region of the Qinghai–Tibet Plateau, unveiled a substantial geothermal resource potential. This breakthrough occurred when temperatures reaching as high as 200 °C were recorded at a depth of 4000 m [10]. Inspired by the discovery of HDR, subsequent geothermal exploration projects and experimental HDR development initiatives were initiated in the basin. Substantial advancements have been achieved thus far. However, the implementation of geothermal exploration projects using multi-hole drilling has revealed that the high-temperature geothermal resources in the Gonghe Basin are not uniformly distributed across the entire basin, but rather occur in localized areas. The discussion on geothermal resources in the Gonghe Basin has been extensive, mainly including research on the geothermal genesis [11–13], thermal structure [13,14], HDR production parameters [10,15,16], and geothermal water chemistry in the basin [17–19]. The current research on geothermal resources in the Gonghe Basin primarily revolves around the thermal reservoir model and the optimization of parameters for HDR development technology. However, there remains a notable dearth of studies concerning the distribution of favorable areas for HDR resources within the basin, the potential quantity of resources, the geological structure of the basin, and its correlation with the spatial distribution of geothermal resources.

The distribution of geothermal resources, specifically hot dry rock (HDR), is widespread, and, theoretically, rocks can be classified as HDR as long as they reach a certain depth and their temperature exceeds 180 °C. However, the estimation of HDR geothermal resource potential is typically limited to areas shallower than 10 km underground, which aligns with the current technological and financial constraints of drilling operations. In other words, the significance of HDR resources lies within this depth range. Building upon the successful HDR development in the Gonghe Basin, there are plans to further explore areas within the basin that exhibit abundant geothermal resources for potential HDR development. Nonetheless, the distribution of geothermal resources in the basin remains uncertain, and the potential for HDR development is unknown. To address this, this paper aims to establish the relationship between the distribution of high-temperature geothermal resources and deep granite in the Gonghe Basin through geophysical exploration, drilling, logging, and thermal source mechanism analysis. By constructing a three-dimensional geothermal geological model, this study seeks to analyze the potential of HDR resources in the Gonghe Basin, thereby facilitating the evaluation of high-temperature geothermal resources and the identification of target areas for future development.

2. Geologic Setting

2.1. Strata and Structure

The Gonghe Basin is located in Qinghai Province, China, to the NE of the Tibetan Plateau (Figure 1). The basin is tectonically controlled by the sinistral strike-slip framework of the Kunlun Orogen and Qinling Orogen to the south and the Qilian Orogen to the north [20]. The Gonghe Basin is surrounded by several faults. To the north, it is bordered by the foothills of the Qinghainan Fault, to the south by the Animaqing Suture Zone (extended from the Kunlun Fault), to the west by the Wahongshan Fault, and to the east by the Duohemao fault. These NNW–SSE and NWW–SEE faults bounding the basin give rise to its conspicuous rhomboid shape.

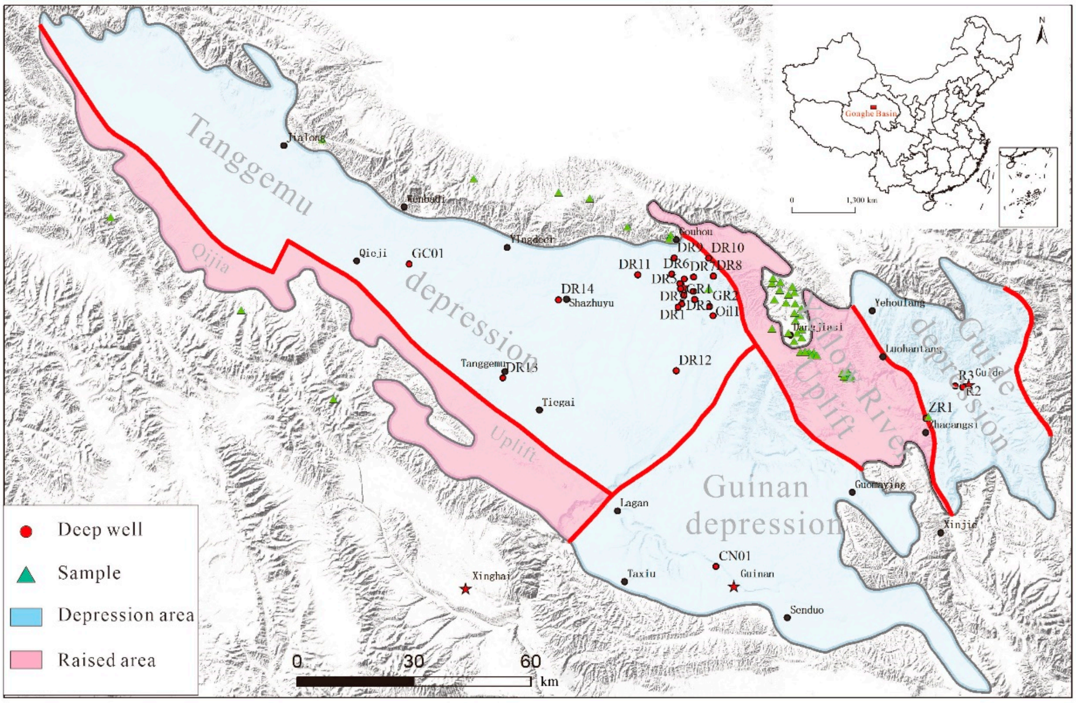

Figure 1. Location of Gonghe Basin and sample collection map (The black dots represent place names).

The area of the Gonghe Basin is approximately 15,200 km^2 [12,21], and the terrain within the basin is flat, with surface elevations of approximately 3000 m. Due to favorable geological conditions for petroleum generation, a series of geophysical exploration works were conducted from the 1970s to the 1990s, which revealed the undulating basement structure. Based on this, the tectonic units of the Gonghe Basin were divided into the Tanggemu depression, Guinan depression, Guide depression, Qijia uplift, and Yellow River uplift. Despite some geophysical exploration work being carried out in the basin, the exact depth of the basement has not yet been determined due to low precision and outdated technology. From 2018 to 2021, a new round of magnetotelluric surveys were conducted in the Gonghe Basin, which have provided a basic understanding of the deep basement depth and tectonic development.

2.2. Thermal Background of Gonghe Basin

The Tibetan Plateau in China is located at the northern margin of the Mediterranean–Himalayan geothermal belts, which are known for their abundant reserves of high-temperature geothermal resources. The surface geothermal heat flow value is relatively high in this region, and various thermal manifestations can be observed at the surface [22]. The most well-known high-temperature geothermal systems include the Yangbajing, Yangyi, and Gudui geothermal systems in southern Tibet, the Rehai geothermal system in western Yunnan, and the Rekeng geothermal system in western Sichuan [23–25]. Compared to the southern region of the Tibetan Plateau, the northeastern region of the plateau has lower heat flow values and has been the focus of comparatively fewer studies on geothermal resources. However, the presence of two high-temperature hot springs within the Gonghe Basin, with temperatures surpassing the local boiling point (92 °C) at 93.5 °C and 96.6 °C, prompted researchers to conduct geothermal drilling within the basin. Surprisingly, during these drilling activities, a HDR reservoir was unexpectedly discovered at a depth of less than 4000 m. This rock body has a temperature of over 180 °C and a geothermal gradient of 41.3 °C/km. The discovery of the HDR greatly boosted the confidence of local workers, and a large number of boreholes were subsequently set up in the Qiabuqia area, Guide area, Guinan area, and Tanggemu area. Through drilling verification, it was found that the geothermal resources in the Gonghe Basin are mainly concentrated in the central and eastern parts and distributed on both sides of the Yellow River Uplift. This finding indicates that HDR bodies are not widespread throughout the basin, but rather occur in localized areas. Additionally, it suggests that the distribution of geothermal resources in the basin may be influenced by the regional basement uplift resulting from the Yellow River Uplift.

3. Three-Dimensional Geological Modeling

There are several methods available for HDR resource assessment, such as the surface heat flux method, heat storage modeling, statistical analysis, and the analogy method [26]. However, the most common methods for estimating geothermal resources are the volume method and the Monte Carlo method [27–30]. The Monte Carlo simulation is a method used for statistically analyzing the probability functions of random events [31]. Although the Monte Carlo method can minimize the uncertainty of parameters, the depth of the strata in the Gonghe Basin is controlled by regional major faults, and the burial depth difference in the same stratum between the upper and lower plates of the fault can reach 6000 m. It is difficult to describe the parameter changes caused by this structural control using the Monte Carlo method. Therefore, this study used the volume method to calculate the HDR resources in the Gonghe Basin. The resource of geothermal energy in HDR is the heat stored in low-porosity and low-permeability rock formations, disregarding the heat-storing capacity of fluids in the rock matrix, as calculated by Equation (1).

$$Q = \rho \cdot C_p \cdot V \cdot (\mathrm{T} - \mathrm{T_c}) \quad (1)$$

where ρ is the density of the rock; C_p is the specific heat of the rock; V is the volume of the rock; T is the temperature of the rock at a specific depth; and $\mathrm{T_c}$ is the reference temperature.

The HDR reservoirs in this study were divided into several calculation units within the first 10 km depth, with a calculation interval of 1 km. The total resource of HDR was calculated by summing up the resource in each layer, as described in Equation (2).

$$Q_T = \sum Q_i \quad (2)$$

where Q_T is the total heat in the HDR reservoir; and Q_i is the heat in the i-th layer of HDR.

The surface of the Gonghe Basin is relatively flat and is generally at an altitude of around 3000 m. However, due to the incision of the Yellow River and the effects of tectonic uplift, the elevation of the basin surface shows a characteristic of being low in the middle and high on the north and south sides. The elevation data of the basin at a 30 m resolution were downloaded for free from the "China DEM Digital Elevation Product" provided by the Computer Network Information Center of the Chinese Academy of Sciences (https://www.gscloud.cn/sources/index?pid=302, accessed on 15 June 2020) and were mosaicked using ArcMap 10.3 (Figure 2). The red line shows the extent of the Gonghe Basin. The river channels that were formed due to the incision of the Shazhuyu River are visible on the surface, and they emerge as surface water in the Dashuiqiao area and merge into the aquifer in the Dalianhai Township on the east. Interestingly, the area labeled "a" in Figure 2 is a 17-level terrace formed by the incision of the Yellow River, which happens to be located on the eastern side where the Shazhuyu River disappears. It is hypothesized that the presence of a fault on the western side leads to a decline in the water table and groundwater level in that area. This decline subsequently contributes to the formation of a sand and gravel aquifer, influenced by the impact of the eastern river flow.

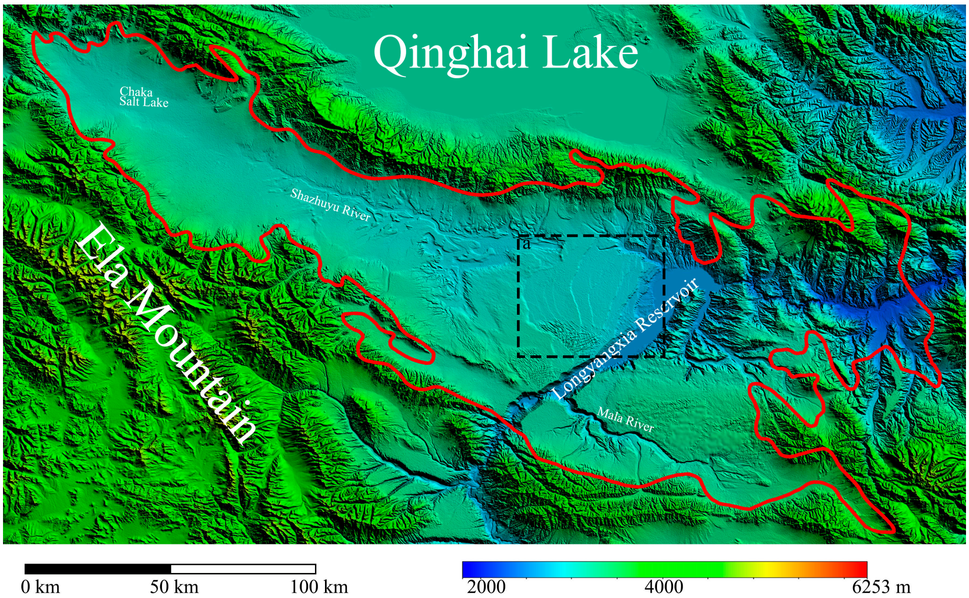

Figure 2. Elevation map of the surface of the Gonghe Basin (a represents the region with developed river terraces.).

The strata in the Gonghe Basin consist of the quaternary Linxia rormation of the upper Eocene, the Xianshuihe formation of the middle Miocene, Xining formation of the late Miocene, and the Triassic basement from top to bottom. The deep basement controls the undulating morphology of the overlying strata. The lithology of the deep basement is mainly composed of an early-to-middle Triassic Longwuhe group of metamorphic sandstone and shale and middle-to-late Triassic granite. The lithology of the underlying rocks differs significantly from that of the overlying sedimentary rocks, and geophysical methods exhibit a relatively high level of accuracy in identifying these differences. Therefore, based on the MT results and constrained by drilling data, the depth of the basement in the Gonghe Basin was mapped (Figure 3). The depth of the basement in the basin is controlled by faults. The F2 fault divides the Tanggemu depression, and the depth of the basement on the western side gradually increases from south to north. The average elevation at the fault contact is about 2000 m. The deepest point of the fault burial depth is 6500 m at the intersection on the western side of the F2 fault. The eastern side of the F2 fault is affected by regional tectonic controls and locally forms folds with slightly higher or lower depths. Generally, the depth of the basement on the eastern side of the Tanggemu depression gradually increases and reaches the surface controlled by the F7 fault. In the Guinan depression, the depth of the basement reaches its maximum in the northwest at the Longyangxia Reservoir and gradually becomes shallower towards the south and east until it reaches the surface. In the Guide depression, the depth of the basement gradually decreases around the Guide County center. The deepest point of the basement in the Guide area is only 1400 m, but small faults are highly developed in this area, groundwater recharge is rapid, and the hydrothermal system is relatively developed.

Based on the depth of the basement in the Gonghe Basin, this study analyzed the morphology of the overlying sedimentary cover. The Xining formation is locally distributed in the Tanggemu depression and was encountered in the GC01 well at a depth of 4005 m. However, the formation was not found in the wells drilled to the east, suggesting possible erosion. The strata in the Chaka area exhibit a relatively stable geological structure characterized by good continuity and the absence of large-scale faults. The reverse faults F4 and F5 are located on the hanging wall and have experienced compression, indicating potential erosion of the Xining formation. Therefore, it is speculated that the Xining formation is developed on the west side of DR14 and the north side of the F5 fault. The Xining formation was encountered in the CN-01 well in the Guinan depression, and there are no large-scale faults in the area. It is inferred that the Xining formation is widely distributed to the east of the F6 fault and in the south of the area. The ZR1, R2, and R3 drill holes in the Guinan depression all encountered the Xining formation, and outcrops are also found in the surrounding mountains, suggesting that the Xining formation is distributed throughout the Guide depression. The Miocene, Pliocene, and Pleistocene sediments in the Gonghe Basin belong to the Tethys Ocean, and their sedimentation is relatively continuous [32]. All boreholes encountered the Linxia and Xianshuihe formations and the above-mentioned formations have a widespread distribution throughout the study area.

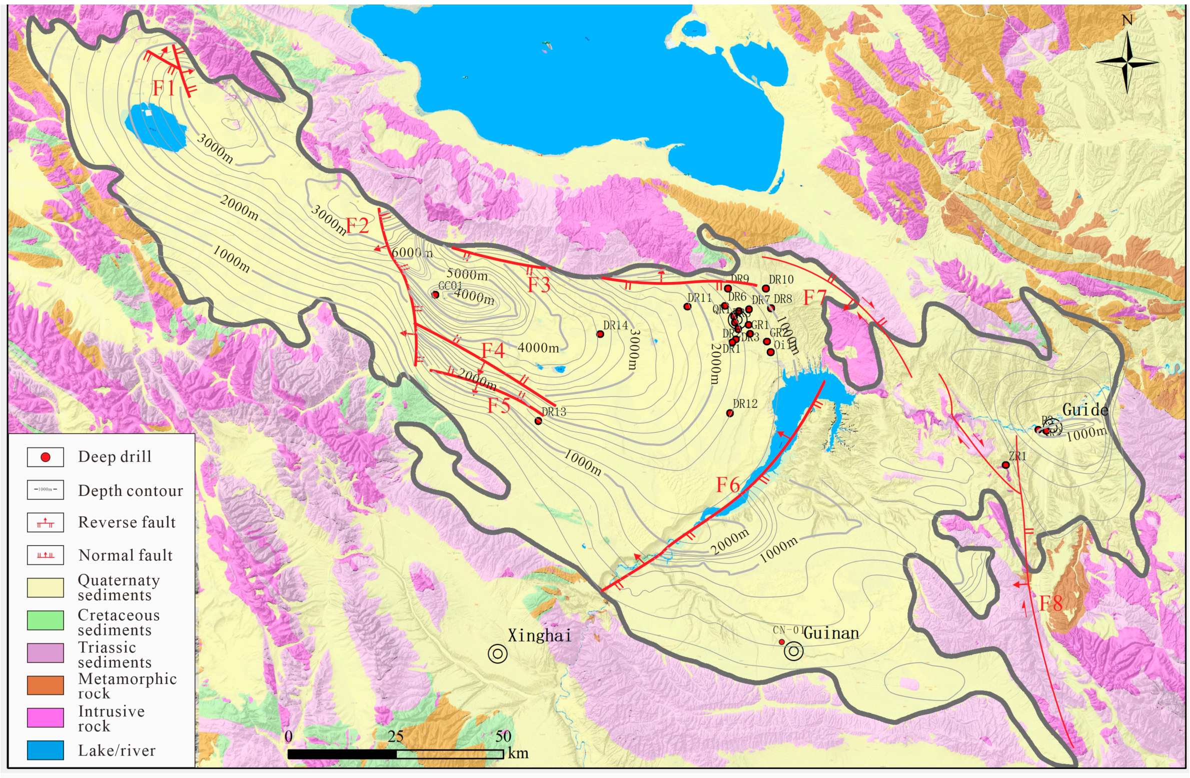

Figure 3. Depth map of the basement in the Gonghe Basin.

The sedimentary cover depth on the eastern side of the Tanggemu depression was determined through high-power time–frequency and two-dimensional seismic surveys. Using the burial depth of sedimentary layers in the Tanggemu area as a reference, the burial depths of the other regions were mapped based on the principle of stratigraphic continuity.

From the revealed stratigraphy through drilling, it is evident that the burial depth of the Linxia formation in well CN-01 is only 293 m (Table 1), which is approximately 300 m shallower compared to the Linxia formation in the northern Tanggemu depression. This is speculated to be due to regional uplift caused by reverse faults in the southern area. Additionally, the Triassic sediments along the fault have experienced uplift, forming mountain ranges (Figure 3 depicts internal faults within the basin, while the fault along the basin boundary is not shown). The uplift magnitude of the stratigraphy increases closer to the fault. However, in the northern part of the CN-01 well, farther away from the fault, the stratigraphy is less affected. In the northern part of the Guinan depression, the burial depth of the sedimentary layers gradually increases until it reaches the Tanggemu depression.

Table 1. Model error statistics table (depth unit: m).

Welllocation	Wellname	Horizons	Real Depth	Model Depth	Error Value	Error Rate
Guide depression	R3	Linxia formation	31	27	4	12.90%
		Xianshuihezu formation	410	399	11	2.68%
		Xiningzu formation	717.3	711.6	5.7	0.79%
		Triassic basement	1400	1394	6	0.43%
	R2	Linxia formation	38.35	32.7	5.65	14.73%
		Xianshuihezu formation	391.45	383.9	7.55	1.93%
		Xiningzu formation	785.85	783.7	2.15	0.27%
		Triassic basement	1490.55	1489.1	1.45	0.10%
	ZR1	Triassic basement	577	566	11	1.91%
Tanggemu depression	GH-01	Linxia formation	546	542	4	0.73%
		Xianshuihezu formation	1034	1031	3	0.29%
		Triassic basement	1360	1356	4	0.29%
	GC01	Linxia formation	1076	1085	−9	0.84%
		Xianshuihezu formation	2447	2456	−9	0.37%
		Xiningzu formation	4005	4053	−48	1.20%
		Triassic basement	5500	5536	−36	0.65%
	DR1	Linxia formation	623	621	2	0.32%
		Xianshuihezu formation	903	902	1	0.11%
		Triassic basement	1302	1302	0	0.00%
	DR2	Linxia formation	504.6	500	4.6	0.91%
		Xianshuihezu formation	906.15	905	1.15	0.13%
		Triassic basement	1406.8	1401	5.8	0.41%
	DR3	Linxia formation	607.5	604	3.5	0.58%
		Triassic basement	1340.25	1337	3.25	0.24%
	DR4	Linxia formation	595.3	593	2.3	0.39%
		Xianshuihezu formation	1011.5	1007	4.5	0.44%
		Triassic basement	1402	1398	4	0.29%
	GR1	Linxia formation	505	504	1	0.20%
		Triassic basement	1350	1347	3	0.22%
	GR2	Linxia formation	270	284	−14	5.19%
		Triassic basement	940	956	−16	1.70%
	QR1	Linxia formation	218.61	224	−5.39	2.47%
		Xianshuihezu formation	532	537	−5	0.94%
		Triassic basement	932.16	945	−12.84	1.38%
	Oil 1	Linxia dormation	169.61	185	−15.39	9.07%
		Xianshuihezu formation	247.87	264	−16.13	6.51%
		Triassic basement	627.88	641	−13.12	2.09%
Guinan depression	GN-01	Linxia formation	293	297	−4	1.37%
		Xianshuihezu formation	725	733	−8	1.10%
		Xiningzu formation	1080	1088	−8	0.74%
		Triassic basement	1137	1146	−9	0.79%

Within the Guide depression, the F8 fault is a significant deep fault that cuts through the Earth's crust. The stratigraphic morphology and burial depth often undergo significant changes near this fault. However, the Guide depression has a small area and is characterized by the presence of three drilled wells, providing relatively abundant stratigraphic data.

The burial depths of various sedimentary layers were mapped based on the exposure of the formations and information obtained from drilling. Based on the above description, 3D models of the various formations in the Gonghe Basin were established, and the morphology of the formations can be seen in Figure 4.

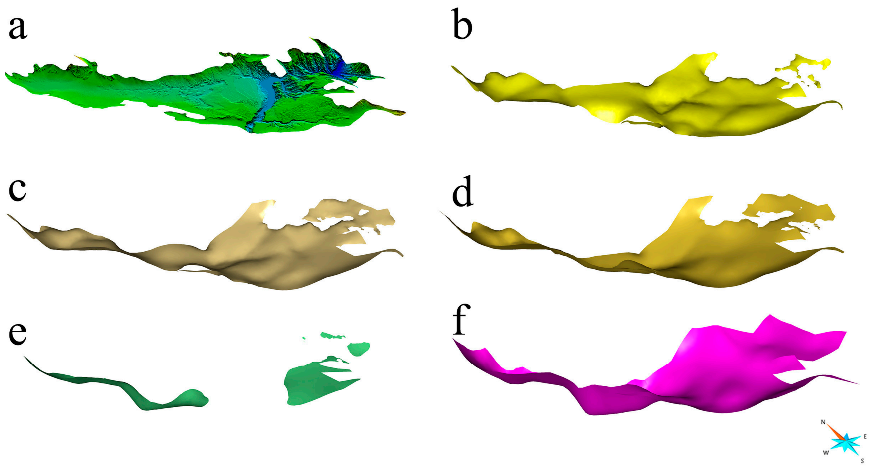

Figure 4. Spatial distribution and morphology map of the Gonghe Basin strata, where (**a**) represents the surface, (**b**) represents the quaternary system, (**c**) represents the Linxia formation, (**d**) represents the Xianshuihe formation, (**e**) represents the Xining formation, and (**f**) represents the basement.

A 3D geological model was constructed for the Gonghe Basin, encompassing a depth of up to 10 km, with the basement being concealed. This approach was adopted due to the distinct shape of the basement in the Gonghe Basin, which is elevated in the north and south while being relatively lower in the central region. This configuration envelops the overlying strata (refer to Figure 4f). Concealing the basement was necessary as it would have otherwise hindered the observation of the morphology of the overlying strata. Figure 5 shows the 3D geological model of the Gonghe Basin, where (a) consists of 9,360,000 partition grids and the lithology, stratigraphic combination, and outcrop distribution are consistent with geological knowledge. The Linxia formation is widely exposed on the surface in the Guide depression, and the exposure of the Xining formation is consistent with its actual location. In the Tanggemu depression and Guinan depression, the surface is covered by quaternary sediments. The Xining formation is partially uplifted due to the thrust faulting of the F4 fault and is then eroded and disappears due to the thrust faulting of the F5 fault. In the eastern part of the basin, such as the Waliguan Mountains, the lithology is mainly Triassic basement, which makes the model look like there is a "hole". Figure 5b shows the geological section of the Gonghe Basin, and it can be observed that the thickness of the overlying strata reaches its maximum value to the east of the F2 fault and gradually decreases to the east and west. The depth of the cover layer in the Guide depression does not exceed 1500 m, and in most areas it is only 600 m, which is why it appears thin in the model. The model agrees with the geophysical exploration results and has a high level of accuracy.

Table 1 juxtaposes the depths of the actual and model stratigraphy. Three wells located in the central zone of the Guide depression were used to constrain the stratigraphic depth, with the model stratigraphic depth generally being shallower than the actual depth (negative error value). This was mainly due to the fact that the Guide depression is sandwiched between the Waliguan Mountains in the west and the Duohemao Mountains in the east, with a difference in height of up to 2000 m between the mountains and the depression. To ensure the continuity and smoothness of the strata, the internal strata in the Guide depression were uplifted to varying degrees. As the Tanggemu depression has the highest number of wells and is the most thoroughly studied area, the error rates for the majority of the strata in the area were relatively small. The highest error rate was found in the Linxia formation in Oil 1, which is located on the western edge of the Yellow River uplift, where the regional strata have been significantly uplifted due to the uplift of the Waliguan Mountains. The Guinan depression had only one well to constrain the stratigraphic depth, but due to small-scale regional faulting, the variation in the strata was small, resulting in a smaller error rate. Overall, the error value between the 3D geological model and the actual stratigraphy in the Gonghe Basin was less than 50 m, and the error rate did not exceed 5% except for some areas with intense structural controls. As a result, the model is considered reliable and can be used to calculate the reserves of geothermal resources.

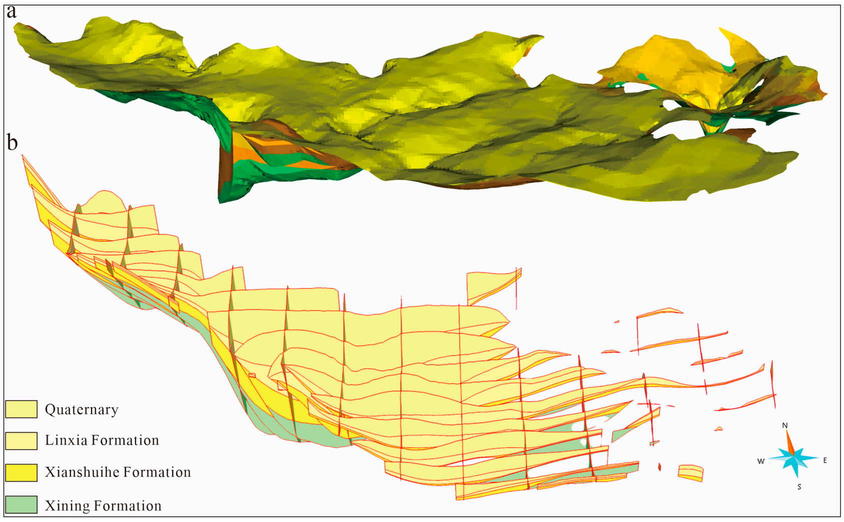

Figure 5. Three-dimensional geological model of the Gonghe Basin. (**a**) represents the 3D diagram of the strata, and (**b**) represents the 3D sliced diagram.

4. Database

4.1. Temperature Logs

The determination of parameter ranges and distribution models is key for the assessment of geothermal resources. Temperature is one of the most important parameters for geothermal resource assessment, and the measurement of a steady-state temperature in boreholes stands as the most direct and efficacious approach for obtaining accurate temperature readings within deeper formations. From 2018 to 2022, the temperature profiles of 24 boreholes were acquired. Thirteen representative boreholes were selected as a reference for temperature calculation, as some of the boreholes were located close to each other. The temperature measurement curves are shown in Figure 6.

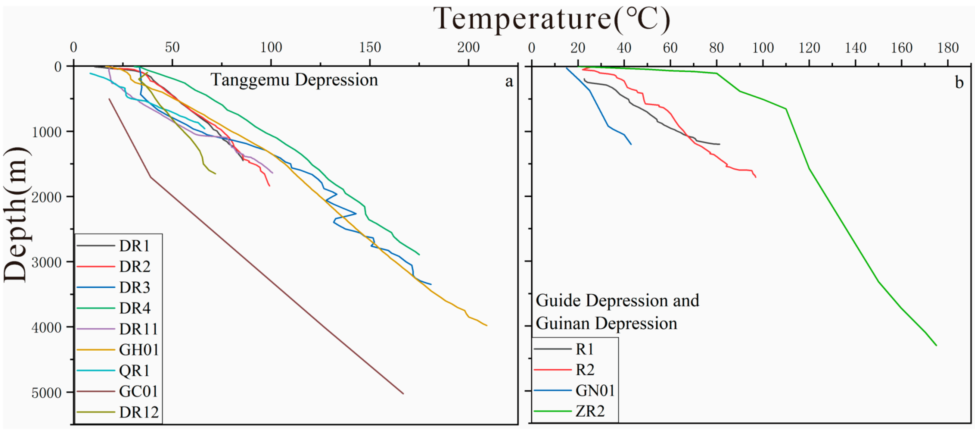

Figure 6. Temperature–depth profile of the Gonghe Basin. (**a**) represents the Tanggemu Depression, and (**b**) represents the Guide and Guinan Depressions.

The temperature measurement curve in the Tanggemu depression can be divided into two parts. The majority of wells, located on the eastern edge of the depression, exhibited higher geothermal gradients. After removing the interference caused by the slight convexity of the convection-type heat storage geothermal gradient curve within 2000 m, the range of the conductive-type heat storage geothermal gradient in the lower portion was found to be between 45 and 50 $^{\circ}C \cdot km^{-1}$. In the Guide depression, a notable characteristic is the considerable strength of shallow convection-type heat exchange, leading to a substantial temperature gradient. However, the geothermal gradient associated with deep conductive-type heat exchange was relatively modest, which was approximately 20–25 $^{\circ}C \cdot km^{-1}$, as determined by comprehensive analysis of the three boreholes. The temperature measurement curve in the Guinan depression showed no influence from shallow convection-type heat exchange, and the geothermal gradient was relatively stable. The calculated geothermal gradient for the conductive storage layer was around 30 $^{\circ}C \cdot km^{-1}$.

4.2. Rock Density

Granite samples were collected from outcrops and drilling wells (Figure 1) in the eastern, northern, and western parts of the Gonghe Basin, and true density tests were conducted. The rocks were dried prior to testing, and the testing was conducted at the Institute of Geology and Geophysics, Chinese Academy of Sciences. The results of the tests are shown in Table 2. The body density of the granite in the Gonghe Basin ranged from 2.53 to 2.99 g/cm^3, with the density of the majority of samples distributed between 2.60 and 2.80 g/cm^3. The granite bodies exposed in the Gonghe Basin were mainly granite and diorite granite, with no significant difference in density. The test results showed that the density of the granite in the basin was relatively uniform. For subsequent calculations of HDR resources, a density average of 2.75 g/cm^3 was set as the calculation parameter based on the test results.

Table 2. Comparison table of sampling points and density of rock samples in Gonghe Basin.

Name	Lithology	Location	Mass (g)	Volume (cm^3)	Density (g/cm^3)
YP01	Granodiorite	Ela Mountain	552.06	205.14	2.69
YP02	Granodiorite	Ela Mountain	69.04	25.45	2.71
YP03	Granodiorite	Ela Mountain	587.46	208.81	2.81
YP04	Granodiorite	Qinghainan Mountain	674.30	260.11	2.59
YP05	Granodiorite	Qinghainan Mountain	448.65	173.36	2.59
YP06	Granodiorite	Qinghainan Mountain	791.21	294.43	2.69
YP07	Monzogranite	Qinghainan Mountain	397.77	154.24	2.58
YP08	Monzogranite	Qinghainan Mountain	472.32	181.73	2.60
YP09	Granodiorite	Qunaihai Gully	15.37	6.02	2.55
YP10	Granodiorite	Qunaihai Gully	48.35	17.36	2.79
YP11	Granodiorite	Qunaihai Gully	30.65	10.71	2.86
YP12	Granodiorite	Qunaihai Gully	52.18	18.85	2.77
YP13	Granodiorite	Qunaihai Gully	69.04	24.89	2.77
YP14	Granodiorite	Qunaihai Gully	47.14	17.46	2.70
YP15	Granodiorite	Qunaihai Gully	53.97	19.43	2.78
YP16	Granodiorite	Qunaihai Gully	54.67	19.94	2.74
YP17	Granodiorite	Qunaihai Gully	24.13	8.58	2.81
YP18	Granodiorite	Qunaihai Gully	78.77	27.87	2.83
YP19	Granodiorite	Qunaihai Gully	17.43	6.18	2.82
YP20	Granodiorite	Qunaihai Gully	52.22	17.88	2.92
YP21	Granodiorite	Qunaihai Gully	50.65	18.06	2.80
YP22	Granodiorite	Reservoir abutment	53.05	19.45	2.73

Table 2. *Cont.*

Name	Lithology	Location	Mass (g)	Volume (cm^3)	Density (g/cm^3)
YP23	Monzogranite	Reservoir abutment	91.99	32.32	2.85
YP24	Monzogranite	Waliguan Mountain	53.97	20.35	2.65
YP25	Granodiorite	Waliguan Mountain	16.17	5.75	2.81
YP26	Granodiorite	Waliguan Mountain	32.71	12.26	2.67
YP27	Monzogranite	Waliguan Mountain	48.11	18.09	2.66
YP28	Granodiorite	Waliguan Mountain	56.46	20.48	2.76
YP29	Granodiorite	Waliguan Mountain	28.10	9.41	2.99
YP30	Granodiorite	Waliguan Mountain	33.26	12.37	2.69
YP31	Granodiorite	Waliguan Mountain	31.50	10.80	2.92
YP32	Granodiorite	Waliguan Mountain	25.20	9.41	2.68
YP33	Granodiorite	Waliguan Mountain	79.45	28.84	2.75
YP34	Granodiorite	Waliguan Mountain	60.42	22.38	2.70
YP35	Granodiorite	Waliguan Mountain	47.00	16.47	2.85
YP36	Granodiorite	Waliguan Mountain	55.12	19.26	2.86
YP37	Granodiorite	Waliguan Mountain	35.10	13.85	2.53
YP38	Granodiorite	Waliguan Mountain	33.74	12.04	2.80
YP39	Monzogranite	Waliguan Mountain	24.26	8.44	2.87
YP40	Monzogranite	Waliguan Mountain	24.38	8.73	2.79
YP41	Monzogranite	Waliguan Mountain	34.48	12.00	2.87
YP42	Monzogranite	Waliguan Mountain	58.03	21.01	2.76
YP43	Monzogranite	Waliguan Mountain	60.00	22.06	2.72

4.3. Specific Heat Capacity of Rocks

The specific heat capacity of a rock quantifies the amount of heat that is either absorbed or released by a unit mass of the material when there is a unit change in temperature. This parameter reflects the amount of heat stored in the rock. The thermal conductivity testing of the rocks was conducted using a differential scanning calorimeter (DSC) with a heat flow configuration. The specific heat capacity testing process involved placing the sample and a reference crucible on a sensor disc to ensure thermal symmetry. Testing was conducted in a uniform furnace following a specific temperature program, including linear heating, cooling, and isothermal stages. A pair of thermocouples continuously measured the temperature difference between the reference and sample. By applying a heat flow correction, the raw temperature difference signal was converted into a heat flow difference signal, and the resulting DSC (differential scanning calorimetry) curve was plotted over time/temperature. Although perfect thermal symmetry was not achievable, the baseline on the DSC curve represented the signal difference between the reference and sample ends, with any deviations known as "baseline drift", reflecting changes in the heat capacity. The tests were performed at temperatures ranging from 25–500 °C under atmospheric pressure with an accuracy of ±1%. The specific heat capacity of a rock varies with temperature. To obtain the specific heat capacity of rocks at different temperatures, this study tested the specific heats of 38 rock samples at temperatures ranging from 25 °C to 190 °C and extracted 14 sets of data to analyze the variation trend of the specific heat capacity with temperature (Figure 7). In the figure, "MO" represents monzogranite, while "GR" represents granodiorite. Based on the rock types, monzogranite and granodiorite showed no significant difference in specific heat capacity. At 25 °C, the specific heat capacity ranges were determined to be 0.79939–0.93198 J/(g·°C) for monzogranite and 0.7968–0.93882 J/(g·°C) for granodiorite. The upper and lower limits of the specific heat capacity were relatively close, indicating that subsequent specific heat assignments do not need to be differentiated based on the rock types. The specific heat capacity of all the samples showed the same increasing trend with temperature, with an increasing amount that gradually decreased. The statistical analysis yielded the following empirical formula.

$$Cp = 0.0614\ln(\mathrm{T}) + 0.8536 \tag{3}$$

where *Cp* represents the specific heat capacity of the rock, and T represents the temperature of the rock at a specific depth.

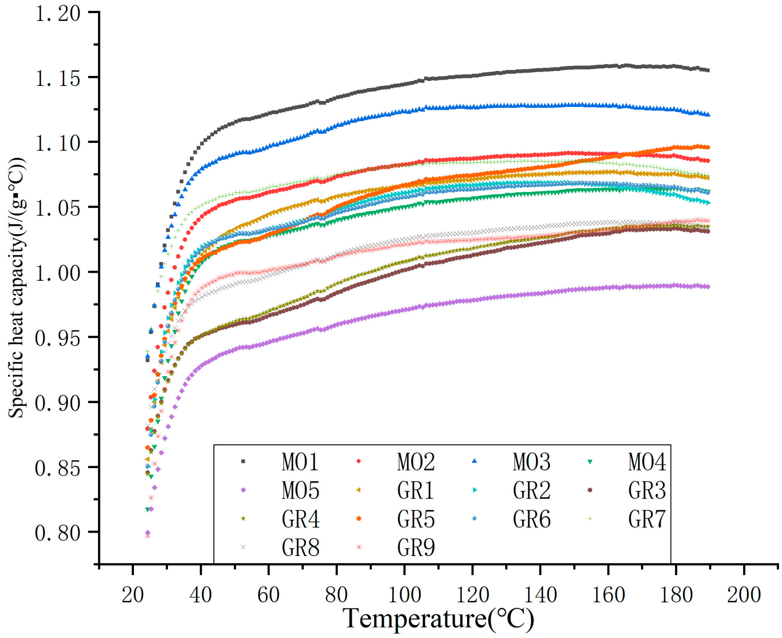

Figure 7. Variation in specific heat capacity of rocks with temperature (25 °C~190 °C).

5. Results

5.1. Selection of HDR Development Target Areas

Based on the thermal properties of the rocks and the regional temperature field data, a distribution pattern of HDR in the Gonghe Basin was created using continuous interpolation methods (Figure 8). HDR was mainly distributed in the eastern part of the basin, with the shallowest depth of about 3500 m and a gradually increasing depth towards the periphery in an elliptical shape. The temperature gradient in this particular area was notably the highest, averaging approximately 52 °C/km. In contrast, the temperature gradient in other regions was typically around 30 °C/km. These findings indicate the significant potential for the development of HDR in the eastern part of the basin, while the western region exhibited relatively limited geothermal resource conditions. Therefore, the red area in Figure 8 was designated as a favorable area for the development of HDR in this study.

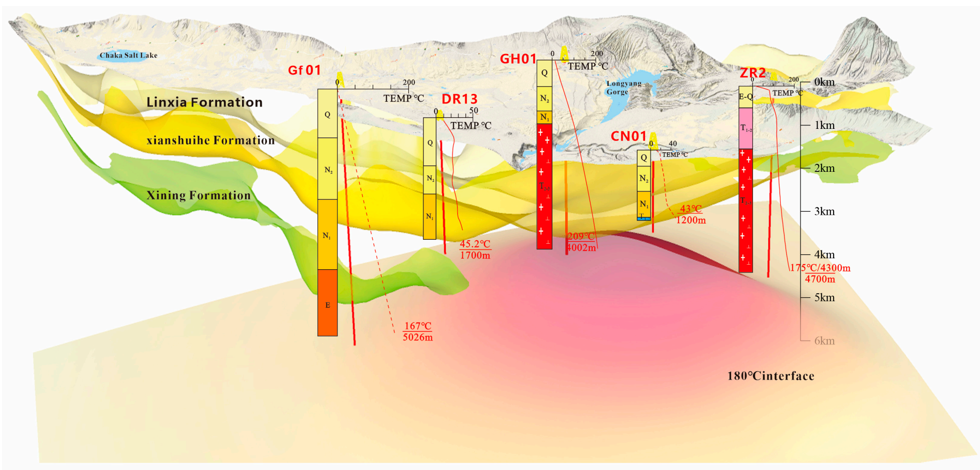

Figure 8. Three dimensional model of the distribution of the HDR body.

5.2. Calculation of HDR Resources in the Gonghe Basin

The relevant data were imported into a three-dimensional geological modeling software program, and Formulas (1) and (2) were used to calculate the HDR resources from a 0 to 10 km depth, along with the saved standard coal amount and reduced emissions of environmental pollutants. The installed capacity represents the amount of available heat energy that can be converted into electricity over the 30-year lifespan of the power plant; the formula for its calculation is shown in Formula (4). The capacity factor (F_c) is defined as the ratio of the actual electricity generation during a certain period to the power generation of the power plant at its rated capacity during the same period. The capacity factor of geothermal power plants is higher than that of other types of power plants and is the highest among all renewable energy power plants. Assuming a capacity factor of 0.90:

$$W = \eta_T \cdot Q_{\mathrm{i}} / \mathrm{t} \cdot F_c \tag{4}$$

where Q_{i} represents the available heat energy per 1 km thick rock layer; η_T is the efficiency of converting heat energy into electricity; t is the number of seconds in 30 years; and F_c represents the capacity factor.

The efficiency of converting heat energy into electricity (η_T) depends on the temperature of the HDR formation and is calculated using Formula (5) [33].

$$\eta_T = 0.000484\mathrm{T}(^{\circ}\mathrm{C}) - 0.0051 \tag{5}$$

The resource potential of the Gonghe Basin is enormous (Table 3). The total volume of HDR within a 10 km depth is 8.11×10^{13} m^3, equivalent to a geothermal resource of 4.90×10^{22} J. If all of this resource can be developed, it would greatly help to alleviate environmental pollution. However, as analyzed earlier, the favorable development targets of HDR are mainly distributed in the eastern part of the basin, where the depth is shallow, the geothermal gradient is high, and the development cost is low. Conversely, when compared to other areas within the basin, the cost of development is higher. Currently, under the existing technological conditions, large-scale development is not yet feasible. HDRs at depths of 3–5 km are more valuable to develop. Based on these calculations, the total volume of HDR within 3–5 km depth in the basin is 6.7×10^{12} m^3, equivalent to a geothermal resource of 2.48×10^{21} J. If a power plant with an installed capacity of 2.94×10^{11} W operates for 30 years, the equivalent standard coal content would be 8.45×10^{10} t. In total, it would reduce CO_2 emissions by 2.21×10^{11} t, SO_2 emissions by 7.18×10^8 t, and NO_x emissions by 6.25×10^8 t.

Table 3. Theoretical geological resource storage of HDR in the Gonghe Basin.

Depth (km)	Volume of HDR (m^3)	HDR Resource Quantity (J)	Installed Capacity (w)	Equivalent Standard Coal Content (t)	Reduction in CO_2 Emissions (t)	Reduction in SO_2 Emissions (t)	Reduction in SO_2 Emissions (t)
3~4	1.20×10^{11}	3.12×10^{19}	3.01×10^{9}	1.06×10^{9}	2.78×10^{9}	9.02×10^{6}	7.85×10^{6}
4~5	6.58×10^{12}	2.45×10^{21}	2.91×10^{11}	8.34×10^{10}	2.19×10^{11}	7.09×10^{8}	6.17×10^{8}
5~6	1.28×10^{13}	6.06×10^{21}	8.39×10^{11}	2.06×10^{11}	5.40×10^{11}	1.75×10^{9}	1.53×10^{9}
6~7	1.51×10^{13}	8.40×10^{21}	1.30×10^{12}	2.86×10^{11}	7.49×10^{11}	2.43×10^{9}	2.12×10^{9}
7~8	1.51×10^{13}	9.44×10^{21}	1.59×10^{12}	3.21×10^{11}	8.42×10^{11}	2.73×10^{9}	2.38×10^{9}
8~9	1.57×10^{13}	1.08×10^{22}	1.96×10^{12}	3.69×10^{11}	9.66×10^{11}	3.13×10^{9}	2.73×10^{9}
9~10	1.57×10^{13}	1.18×10^{22}	2.28×10^{12}	4.01×10^{11}	1.05×10^{12}	3.41×10^{9}	2.97×10^{9}
Total	$\mathbf{8.11 \times 10^{13}}$	$\mathbf{4.90 \times 10^{22}}$	$\mathbf{8.26 \times 10^{12}}$	$\mathbf{1.67 \times 10^{12}}$	$\mathbf{4.37 \times 10^{12}}$	$\mathbf{1.42 \times 10^{10}}$	$\mathbf{1.23 \times 10^{10}}$

It is evident that the Gonghe Basin possesses vast reserves of HDR resources with tremendous development and utilization potential. However, the distribution of geothermal resources is uneven. Based on the results of this study, it is recommended that future geothermal exploration and development in the Gonghe Basin focus on three aspects.

First, it is advisable to implement HDR development in the eastern part of the basin, where there is a high geothermal gradient and a shallow burial depth of HDR. Additionally, during development, it is recommended to consider the simultaneous utilization of overlying Linxia formation and Xianshuihe formation geothermal water (with a temperature of approximately 70 °C) to maximize the cascaded use of geothermal resources.

Second, although this study depicted the depth of the 180 °C isothermal surface through three-dimensional geological modeling, the deep heat convergence pathways in the Gonghe Basin are still uncertain. Hence, it is recommended to conduct targeted investigations on the heat convergence patterns of HDR in future studies.

Third, the relationship between the extractable resource volume of HDR and the overall geothermal resource potential is not yet clear. The existing methods primarily rely on numerical simulations to determine this relationship. Currently, the Gonghe Basin is implementing an EGS project. Subsequent analysis will combine the evaluated geothermal resource potential with the measured extractable resource volume to investigate the relationship between the two.

By focusing on these three aspects, further geothermal exploration and development in the Gonghe Basin can be conducted in a more targeted and efficient manner, maximizing the utilization of its HDR resources.

6. Conclusions

Through the analysis and integration of various data sources in the Gonghe Basin, a three-dimensional geological model of the basin was established to support subsequent exploration, drilling, and geophysical survey work. By using the three-dimensional geological model, the eastern part of the Gonghe Basin was identified as a favorable development area for HDR with a shallow depth (~3500 m) and a high geothermal gradient (>52 $°C \cdot km^{-1}$). In contrast, the western part of the basin has deeper depths and a lower potential for the development and utilization of HDR. By establishing a thermal and physical database for HDR in the Gonghe Basin, it was estimated that the total resource of HDR at depths of 3–10 km in the basin is approximately 4.90×10^{22} J, equivalent to 1.67×10^{12} t of standard coal. The estimated value for HDR with development potential at depths of 3–5 km is approximately 2.48×10^{21} J, equivalent to 8.45×10^{10} t of standard coal.

Author Contributions: Formal analysis, G.Z.; Investigation, Z.D., Q.F., Z.N. and W.X.; Supervision, L.Z. All authors have read and agreed to the published version of the manuscript.

Funding: This study was supported by the Open Project Program of the Key Laboratory of Groundwater Resources and Environment (Jilin University), Ministry of Education (Grant No. 202207007KF), the National Natural Science Foundation of China (42202336), China Geological Survey Project (DD20230018), and Guizhou Provincial Bureau of Geology and Mineral Resources Research Project (No. [2022]01).

Data Availability Statement: Not applicable.

Conflicts of Interest: The authors declare no conflict of interest.

References

1. Lund, J.W.; Toth, A.N. Direct utilization of geothermal energy 2020 worldwide review. *Geothermics* **2021**, *90*, 101915. [CrossRef]
2. Guiling, W.; Wenjing, L.; Wei, Z.; Chuan, L.; Feng, M.; Haonan, G. Research on Formation Mechanisms of Hot Dry Rock Resources in China. *Acta Geol. Sin.* **2016**, *90*, 1418–1433. [CrossRef]
3. International Energy Agency. *IEA Technology Roadmaps Technology Roadmap: Geothermal Heat and Power*; Complete Edition; OECD Energy: Paris, France, 2011; ISBN 9789264118485.
4. Schill, E.; Genter, A.; Cuenot, N.; Kohl, T. Hydraulic performance history at the Soultz EGS reservoirs from stimulation and long-term circulation tests. *Geothermics* **2017**, *70*, 110–124. [CrossRef]

5. Potter, R.; Robinson, E.; Smith, M. Method of Extracting Heat from Dry Geothermal Reservoirs. U.S. Patent 3,786,858, 22 January 1974.
6. Jiyang, W.; Hu, S.; Pang, Z.; He, L.; Ping, Z.; Zhu, C.; Song, R.; Tang, X.; Kong, Y.; Lu, L.; et al. Estimate of Geothermal Resources Potential for Hot Dry Rock in the Continental Area of China. *Sci. Technol. Rev.* **2012**, *30*, 32.
7. Brown, D. *Review of Fenton Hill HDR Test Results*; Los Alamos National Laboratory (LANL): Los Alamos, NM, USA, 1997.
8. Grigoli, F.; Cesca, S.; Rinaldi, A.P.; Manconi, A.; López-Comino, J.A.; Clinton, J.F.; Westaway, R.; Cauzzi, C.; Dahm, T.; Wiemer, S. The November 2017 M w 5.5 Pohang earthquake: A possible case of induced seismicity in South Korea. *Science* **2018**, *360*, 1003–1006. [CrossRef]
9. Jung, R. EGS—Goodbye or Back to the Future 95. *Br. J. Diabetes Vasc. Dis.* **2013**, *2*, 153–155.
10. Zhang, C.; Jiang, G.; Jia, X.; Li, S.; Zhang, S.; Hu, D.; Hu, S.; Wang, Y. Parametric study of the production performance of an enhanced geothermal system: A case study at the Qiabuqia geothermal area, northeast Tibetan plateau. *Renew. Energy* **2019**, *132*, 959–978. [CrossRef]
11. Xue, G.; Qian, H.; Jiang, M.; Su, H. Studies on the velocity structure of crust-upper mantle beneath Northeast Qinghai-Tibet Plateau, China. *Acta Geosci. Sin.* **2003**, *24*, 19–26.
12. Yan, W. Characteristics of Gonghe Basin hot dry rock and its utilization prospects. *Sci. Technol. Rev.* **2015**, *33*, 54–57.
13. Zhang, C.; Hu, S.; Zhang, S.; Li, S.; Zhang, L.; Kong, Y.; Zuo, Y.; Song, R.; Jiang, G.; Wang, Z. Radiogenic heat production variations in the Gonghe basin, northeastern Tibetan Plateau: Implications for the origin of high-temperature geothermal resources. *Renew. Energy* **2020**, *148*, 284–297. [CrossRef]
14. Zhang, C.; Huang, R.; Qin, S.; Hu, S.; Zhang, S.; Li, S.; Zhang, L.; Wang, Z. The high-temperature geothermal resources in the Gonghe-Guide area, northeast Tibetan plateau: A comprehensive review. *Geothermics* **2021**, *97*, 102264. [CrossRef]
15. Xu, T.; Yuan, Y.; Jia, X.; Lei, Y.; Li, S.; Feng, B.; Hou, Z.; Jiang, Z. Prospects of power generation from an enhanced geothermal system by water circulation through two horizontal wells: A case study in the Gonghe Basin, Qinghai Province, China. *Energy* **2018**, *148*, 196–207. [CrossRef]
16. Zhong, C.; Xu, T.; Gherardi, F.; Yuan, Y. Comparison of CO_2 and water as working fluids for an enhanced geothermal system in the Gonghe Basin, northwest China. *Gondwana Res.* **2022**, *in press*. [CrossRef]
17. Zhang, X.; Guo, Q.; Liu, M.; Luo, J.; Yin, Z.; Zhang, C.; Zhu, M.; Guo, W.; Li, J.; Zhou, C. Hydrogeochemical processes occurring in the hydrothermal systems of the Gonghe–Guide basin, northwestern China: Critical insights from a principal components analysis (PCA). *Environ. Earth Sci.* **2016**, *75*, 1187. [CrossRef]
18. Hou, Z.; Xu, T.; Li, S.; Jiang, Z.; Feng, B.; Cao, Y.; Feng, G.; Yuan, Y.; Hu, Z. Reconstruction of different original water chemical compositions and estimation of reservoir temperature from mixed geothermal water using the method of integrated multicomponent geothermometry: A case study of the Gonghe Basin, northeastern Tibetan Plateau, China. *Appl. Geochem.* **2019**, *108*, 104389.
19. Cao, W.-G.; Yang, H.-F.; Liu, C.-L.; Li, Y.-J.; Bai, H. Hydrogeochemical characteristics and evolution of the aquifer systems of Gonghe Basin, Northern China. *Geosci. Front.* **2018**, *9*, 907–916. [CrossRef]
20. Fang, X.; Yan, M.; Van der Voo, R.; Rea, D.K.; Song, C.; Parés, J.M.; Gao, J.; Nie, J.; Dai, S. Late Cenozoic deformation and uplift of the NE Tibetan Plateau: Evidence from high-resolution magnetostratigraphy of the Guide Basin, Qinghai Province, China. *GSA Bull.* **2005**, *117*, 1208–1225. [CrossRef]
21. Zhang, E.-Y.; Survey, C.G.S.C.F.H.A.E.G.; Wen, D.-G.; Wang, G.-L.; Yan, W.-D.; Wang, W.-S.; Ye, C.-M.; Li, X.-F.; Wang, H.; Tang, X.-C.; et al. The first power generation test of hot dry rock resources exploration and production demonstration project in the Gonghe Basin, Qinghai Province, China. *China Geol.* **2022**, *5*, 372–382. [CrossRef]
22. Tian, J.; Pang, Z.; Wang, Y.; Guo, Q. Fluid geochemistry of the Cuopu high temperature geothermal system in the eastern Himalayan syntaxis with implication on its genesis. *Appl. Geochem.* **2019**, *110*, 104422. [CrossRef]
23. Wang, Y.; Guo, Q. The Yangbajing geothermal field and the Yangyi geothermal field: Two representative fields in Tibet, China. In Proceedings of the World Geothermal Congress, Bali, Indonesia, 25–29 April 2010.
24. Tian, J.; Pang, Z.; Guo, Q.; Wang, Y.; Li, J.; Huang, T.; Kong, Y. Geochemistry of geothermal fluids with implications on the sources of water and heat recharge to the Rekeng high-temperature geothermal system in the Eastern Himalayan Syntax. *Geothermics* **2018**, *74*, 92–105. [CrossRef]
25. Wang, C.; Zheng, M. Hydrochemical Characteristics and Evolution of Hot Fluids in the Gudui Geothermal Field in Comei County, Himalayas. *Geothermics* **2019**, *81*, 243–258. [CrossRef]
26. Wang, Y.; Wang, L.; Bai, Y.; Wang, Z.; Hu, J.; Hu, D.; Wang, Y.; Hu, S. Assessment of Geothermal Resources in the North Jiangsu Basin, East China, Using Monte Carlo Simulation. *Energies* **2021**, *14*, 259. [CrossRef]
27. Muffler, P.; Cataldi, R. Methods for regional assessment of geothermal resources. *Geothermics* **1977**, *7*, 53–89. [CrossRef]
28. Wang, Z.; Jiang, G.; Zhang, C.; Tang, X.; Hu, S. Estimating geothermal resources in Bohai Bay Basin, eastern China, using Monte Carlo simulation. *Environ. Earth Sci.* **2019**, *78*, 355.1–355.13. [CrossRef]
29. Zheng, H.; Yiqiao, C.; Shufang, W.; Xiao, L.; Ying, S. Geothermal Resource Assessment based on Monte-Carlo Method—A Case Study of Geothermal Field in Xiong County of Hebei Province. *Urban Geol.* **2015**, *4*, 58–62.
30. Shah, M.; Vaidya, D.; Sircar, A. Using Monte Carlo simulation to estimate geothermal resource in Dholera geothermal field, Gujarat, India. *Multiscale Multidiscip. Model. Exp. Des.* **2018**, *1*, 83–95. [CrossRef]

31. Arkan, S. Assessment of Low Temperature Geothermal Resources. Master's Thesis, Middle East Technical University, Ankara, Turkey, 2003.
32. Craddock, W.H. Structural and Geomorphic Evolution of the Gonghe Basin Complex, Northeastern Tibet: Implications for the Timing of Plateau Growth. Ph.D. Thesis, The Pennsylvania State University, State College, PA, USA, 2011.
33. Tester, J.W.; Anderson, B.J.; Batchelor, A.S.; Blackwell, D.D.; DiPippo, R.; Drake, E.M.; Garnish, J.; Livesay, B.; Moore, M.; Nichols, K. The future of geothermal energy. *Mass. Inst. Technol.* **2006**, *358*, 1–3.